ELSEVIER

Contents lists available at ScienceDirect

## Reliability Engineering and System Safety

journal homepage: www.elsevier.com/locate/ress





# A moment-matching method for fragility analysis of transmission towers under straight line winds

Saransh Dikshit<sup>a</sup>, Alice Alipour<sup>b,\*</sup>

- <sup>a</sup> Iowa State University of Science and Technology: Iowa State University, Ames, IA, United States
- b Iowa State University, Ames, IA, United States

#### ARTICLE INFO

#### Keywords: Transmission towers Straight-line wind Fragility analysis Moment matching technique

#### ABSTRACT

Failure of a transmission line system due to extreme weather conditions such as derechos, hurricanes, and other extreme wind events has caused major widely spread outages. While determining the probability of failure for transmission line components due to such wind events is an important first step for assessing the risk associated with system failure and system resilience, development of fragility functions can be a tedious task because of uncertainties associated with structure, line span, and loading. This paper presents a novel moment-matching technique for handling such uncertainties and estimating the structural fragility of a transmission tower system. Limit states are identified by carrying out nonlinear buckling analysis. Wind-load models are capable of accounting for coherence along the horizontal and vertical directions, after which fragility analysis for the transmission tower system can be carried out by considering variability in structural parameters and wind loads. Realistic drag coefficients were employed for analysis based on wind-tunnel tests carried out for the case-study tower system. The effects of adjacent towers was also considered to account for more realistic boundary conditions. Fragility curves for different wind directions are presented for two states of a system that includes a transmission line system with balanced loads (i.e., intact) and one with unbalanced forces (i.e., with broken conductors).

#### 1. Introduction

Electrical transmission systems, integral parts of the electric power network, are highly susceptible to threats from natural or human-made hazards. Possible failures of transmission towers and lines and associated massive area blackouts could pose severe threats to power system security, a great challenge for the stakeholders, decision-makers, and communities they serve. In the Americas and Australia, approximately 80% of transmission-tower failures are associated with strong wind loadings from tornados, hurricanes, or thunderstorms [1-5]. For example, more than five million people in the U.S. west coast lost power on December 22, 1982, after high winds knocked over a 500-kV transmission tower that then fell into a parallel 500-kV line tower. The failure mechanically cascaded and caused three additional towers to fail on each line [3]. The June 2012 Derecho in the District of Columbia and Canada resulted in 4.2 million people losing power, while outages in 11 Midwest and Mid-Atlantic states and the District of Columbia were also related to strong winds and associated with tree-falling and wire-breakage under extreme weather conditions [6]. More recently, the August 2020 Midwest derecho caused an estimated 1.4 million simultaneous outages. To avoid future transmission tower system failures and achieve quick recovery in susceptible areas from future extreme wind events, understanding the structural capacity and the characteristics of interactions between transmission tower systems and strong winds are essential for system safety and reliability.

Various applications of probabilistic methods in engineering that incorporate reliability and fragility analysis offer a methodical approach to studying the probability of failure of various structures, while considering the uncertainties associated with all the variables involved in the performance of those structures. During the last decades, many organizations such as the International Electrical Commission (IEC), the Institute of Electrical and Electronic Engineers (IEEE) [7,8], and the American Society of Civil Engineers (ASCE) introduced and employed reliability-based design methods to transmission-line design. As a result, many reliability-based design ideas and concepts, such as the North-American Standard ASCE 74 [9], the European Standard EN 50341 [10], CEI/IEC 60826 [11], and CAN/CSA-C22.3 [12] were developed. Since then, structural system reliability analysis of

E-mail address: alipour@iastate.edu (A. Alipour).

<sup>\*</sup> Corresponding author.

transmission lines has become an essential method used in designing new lines and in evaluating or upgrading existing lines [13–17].

In these codes or design manuals, an orthogonal approach is used to model transmission-tower wind loads as loads in the transverse and longitudinal directions. However, with a significant difference in wind drag forces in different wind directions, wind loads could significantly differ from those defined in the codes [18]. Most such codes [9-12] use a global approach to estimate the loads on lattice towers. This method is based on the solidity ratio of the lattice structure, the ratio of the projected area to the total area, a measure of the obstruction and flow momentum loss caused by the lattice structure. Primary sources in wind engineering, including [19] and few design codes (e.g., IEC), provide equations that are adopted from earlier tests that relate the solidity ratio to the tower orientation angle (e.g., [20-22]). However, because of the irregular shapes of these towers, using one solidity ratio for the whole tower introduces a great extent of uncertainty or inaccuracy. The method ends up using the same drag coefficient for the truss of a certain solidity ratio regardless of different wind directions it may experience. Furthermore, the drag coefficients for two truss segments that look different but have the same solidity ratio are taken to be the same. This procedure does not adequately demonstrate the wind-structure interactions for different structural geometries and it tends to lead to erroneous results for the structural behavior of the system. In addition, due to the broad geographic spread of transmission line systems as well as interaction between the tower and the conductors, the localized characteristics of wind environments, wind profiles, and time histories could be different for different sites with different meteorological data. A review of the literature shows that the aerodynamic coefficients for different configurations of transmission towers are rarely available [23]. A few researchers have attempted to develop local approaches with the wind forces evaluated under straight-line conditions on each truss member separately, then summed up to assess the total wind forces exerted on the structure [24,25]. The method, although promising, has been shown to render infeasible results foor a variety of transmission towers with hundreds of truss members with different orientations and alignments. This underscores the need for a more accurate estimation of the loads across the lattice structure of transmission towers.

To assess the risk posed to the transmission power system, including the transmission towers and the conductors, it is essential to evaluate the structural performance in multiple limit states for different failure modes. A practical methodology would be to include the associated uncertainties from the structure and the surrounding environment and build fragility functions for the structural system for risk analysis. Fu et al. [26] developed fragility curves for transmission towers subject to wind loading while considering the uncertainty of the wind only. Park et al. [27] calculated seismic fragility curves of high-voltage transmission towers using a deterministic structural model. Yang and Hong [28] assessed the capacity curve of a tower-line system considering the interactions of turbulent winds and tower wires, with results that showed that turbulent winds introduced variability in the capacity curve. Fu and Li [29] presented an uncertainty analysis method for tower structures subject to wind loading that involved uncertainties of material properties and geometric dimensions. More recently, work done by Tian et al. [30] also focused on the collapse mechanism and fragility analyses of a typical long-span transmission tower-line system under wind loads. A new index, the Global Damage Index (GDI), was proposed for estimating the collapse of the system, and it was further used to generate fragility curves for a transmission tower system subjected to different wind directions. These studies considered either variability in the wind loading along the height of the structure or variability of material characteristics, while horizontal variation in wind loading across the span of the transmission line was not accounted for. A few recent studies have also focused on the implications on system level reliability of fragility curves for transmission tower systems under hurricanes or strong wind events, and have also highlighted the need in estimating system reliability for accounting for interactions among

different transmission tower systems components [31-35]. Another common practice for those considering the probabilistic nature of the wind was use of computationally-intensive Monte Carlo Simulation (MCS) techniques, significantly increasing the number of simulations required and resulting in studying only a limited number of cases. Another daunting task in developing fragility functions for transmission line systems is the inherent, implicit nature of limit-state functions for each structural component comprising the system. This condition makes it challenging to implement gradient-based reliability analysis methods [36,37] that require estimation of the gradient of the performance function. Simulation-based methods [38,39] would also be unfeasible and challenging to perform given the time and computational effort needed for repeated evaluations using complex and detailed finite-element models. There is thus a need to efficiently present limit states for a tower line system that considers different failure modes of the system and can be readily used to assessing system performance.

This paper presents a probabilistic framework for fragility analysis of electric transmission-tower systems subjected to dynamic wind loads. It addresses the identified gaps in modeling of the effect of adjacent spans on the tower of interest, the wind loading along the tower, the wind variation along the tower and across spans, and the variability introduced by material properties. For this purpose, an equivalent system has been developed to represent the effects of neighboring spans on the performance of a target tower. Limit states are developed based on nonlinear buckling analysis for the tower-isolator-conductor system considered. Stochastic wind loading is generated for the towerconductor system, including both mean and the fluctuating components not only along the vertical direction (tower height) but also in the horizontal direction (span length of the transmission network). These wind loadings are realistic in nature and help in representing actual behavior of a transmission network under straight-line winds. For calculation of accurate drag loads on the tower cable system, the results from a recent wind tunnel test on the lattice structure [40] and on the conductor [41] were used. The paper is organized into four main sections. In the first section, the structural model is presented and validated with full-scale test-to-failure data. In the second section, nonlinear pushover analysis is carried out for the different configurations to assess the effect of additional spans on the behavior of a tower of interest. In the third section, structural-parameter uncertainty is discussed and nonlinear buckling analysis for the equivalent transmission tower-conductor is carried out to identify the limit states. In the fourth section, stochastic wind fields are generated based on realistic aerodynamic coefficients extracted from a recent experimental study and applied to the equivalent transmission tower system. Nonlinear time-history analysis is then carried out and results presented for the transmission tower system. Finally, fragility curves are obtained for different orientations of the transmission tower network for probabilistic capacity assessment and future integration into a system-level reliability analysis.

#### 2. Finite-element modeling of a transmission tower

The lattice transmission tower in this study is modeled after a 500 kV transmission tower commonly deployed by the Bonneville Power association (BPA) for which test-to-failure data was available to validate the structural model. The finite-element model was built by commercial software ANSYS using 3D beam elements (Beam 188) and truss elements (Link 180) with a total of 3421 elements and 2845 nodes. The four nodes at the ground level are fixed. The leg members of the tower were treated as beam members, and the primary bracing members of the tower were treated as truss members. The lattice structure consists of angle members. Various models can be adopted for constructing the tower geometry that includes the truss, beam, and beam-truss elements. In this study, a beam-truss model is adopted in which the legs and the primary bracings of the tower act as beam and truss members, respectively. The beam elements are based on Timoshenko beam theory. Since each beam

element can translate and rotate in the X, Y, and Z directions, it experiences axial, shear and moment deformations. With respect to the truss element, since it only has translations along the X, Y and Z directions with no rotational degrees of freedom, it is subjected only to axial loading and can deform in the axial direction. By adopting this beamtruss model one can avoid planar joints in the case of a truss model and a higher stiffness model in the case of a beam model. Previous studies have highlighted the effects of joint rigidity in the performance of transmission towers [42]. This paper uses semi rigid joints for modeling the joints, as shown to perform satisfactorily following Lee & McClure [43]. Material non-linearity and the geometric non-linearity are included by using bilinear elastoplastic material properties and by implementing large deformation analysis, respectively.

After defining the material properties and cross sections for all the members, modal analysis was carried out for the tower determine the natural frequencies of the tower and the associated mode shapes. Fig. 1 shows the first three mode shapes along with the corresponding natural frequencies. Based on the modal analysis, the first, second, and third mode are longitudinal, transverse, and torsional and have frequencies of vibration 1.46, 1.50, and 2.93 Hz, respectively. Fig. 1 also presents the overall design of the tower along with the tower dimensions. The transmission tower is divided into panels as shown in Fig. 2. For each of the panels, the different member sections along with their distributions along the longitudinal and transverse directions are also shown in Tables 1 and 2 respectively.

The conductors and insulators were modeled with Link 180 elements that are ideal truss members and can only take tension or compression loads. The cables attached on the side of the tower are based on the catenary equation that consider span length, gravitational effects, and pretension in the cables. These cables or conductors are suspended through an insulator string present on each side of the top part of the transmission tower. The length of the insulator string is 2.3 m with a mass of 8 kg. Table 3 summarizes the properties for the tower and Table 4 summarizes the results for the conductors and insulators. Both these tables depict the material and geometric properties for the tower and cables that comprise the transmission tower system.

In practice, although a finite-element model with three towers and four span lines is normally used to accurately simulate the boundary conditions for the tower of interest in the center [44], this approach leads to poor computational efficiency in the instance of fragility

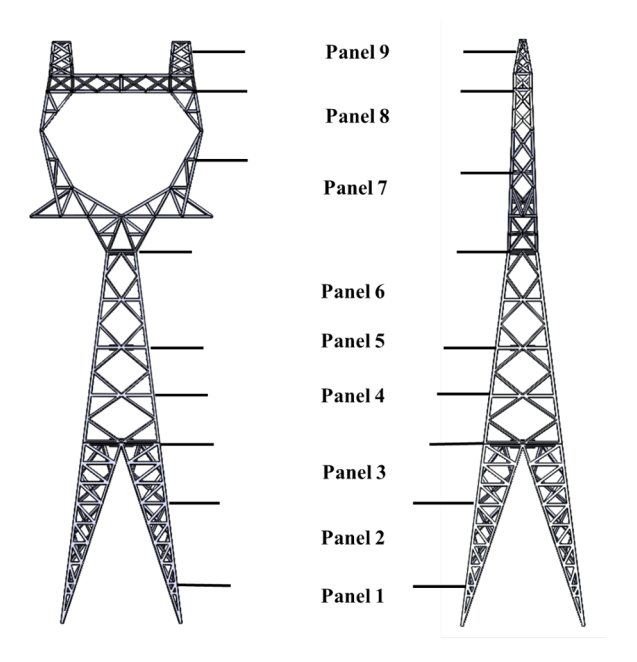


Fig. 2. Panel distribution of transmission tower.

Table 1
Nominal section properties.

Member type	Dimensions (in)	Key
Chords and horizontals	$3.5 \times 3.5 \times 1/4$	a
	$2 \times 2 \times 1/8$	b
	$2 \times 2 \times 3/16$	c
	$3 \times 3 \times 1/4$	d
	$3 \times 3 \times 3/16$	e
Diagonals and legs	$5 \times 5 \times 3/8$	A
	$5 \times 5 \times 5/16$	В
	$4 \times 4 \times 1/4$	C
	$4 \times 4 \times 3/8$	D

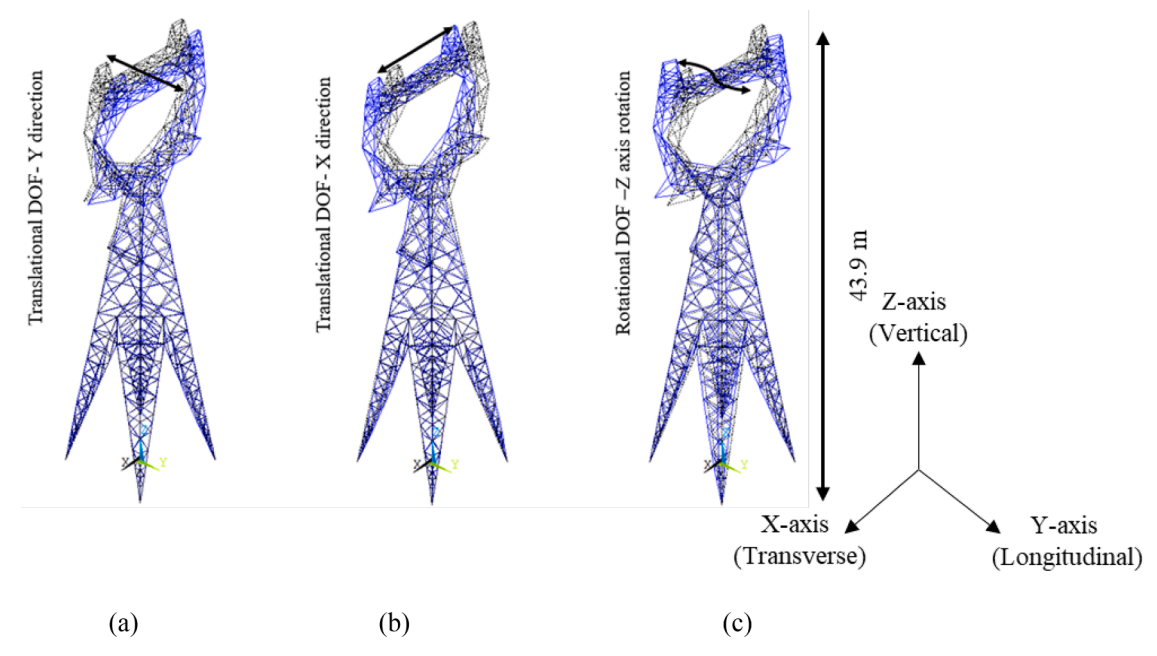


Fig. 1. Modal analysis of the transmission tower (a) longitudinal mode (f = 1.46 Hz); (b) transverse mode (f = 1.50 Hz); (c) torsional mode (f = 2.93 Hz).

**Table 2** Structural steel distribution by panel.

Panel	Members resisting in longitudinal direction	Members resisting in transverse direction
1	A,B,a,c	A, B, a,c
2	A,B,c,d	A,B,a,c
3	A,B,d,e	A,B,c,d
4	A,B,a,d	A,B,a,c
5	A,B,c,d	A,B,a,e
6	A,B,a,c	A,B,a,e
7	C,D,d,e	A,B,a,c
8	C,D,d,e	C,D,e
9	C,D,d,e	C,D,e

**Table 3**Material and geometric properties for the transmission tower.

Component	Tower	
Material	A36 structural steel	
Dimensions	Cross sections assigned based on the structural drawing	
Young's Modulus	200 GPa	
Yield Stress	250 MPa	

**Table 4**Material and geometric properties for conductors and insulators.

Component	Cable	Insulator
Dimensions	0.025 m (outside diameter)	0.34 m (outside diameter)
Young's Modulus	65 GPa	100 GPa
Length	300 m	2.3 m
Density	2.67 kg/m	206.75 kg/m

analysis where a significant number of simulations are required. Also, if only a single tower (tower of interest) is considered, it is imperative during dynamic wind analysis that the adjacent transmission lines also be considered. This results in significantly complex boundary conditions of the cross arm due to the time-varying mechanical properties of the transmission line. Some simplified methods for simulating transmission lines have been proposed to reduce the number of elements, e.g., by simplifying the line as a rigid link or a spring [45]. However, since these methods cannot accurately simulate the boundary conditions of the cross-arm, a simplified model consisting of a transmission line with one tower and two span lines consisting of springs at boundary conditions is adopted herein, based on the work done by [44] that solves the issue of accurately modeling the boundary conditions at the cross-arm location. The springs are meant to mimic the mechanical behavior of the complex system in a simplified model. A preliminary study was first conducted to study the importance of the towers and conductors present on adjacent sides of the tower of interest. The simplified boundary condition adopted for the transmission line is shown in Fig. 3. The conductor is suspended by a cross arm through an insulator string on the tower. The upper node of the insulator string is constrained by the cross-arm and can be regarded as a pinned connection. The parameters k<sub>tcx</sub> and k<sub>tcv</sub>, calculated through finite element analysis of the complex system, represent the stiffnesses of the cross-arms in the two horizontal directions, respectively. In the simplified method, since the adjacent conductors have been eliminated, a horizontal spring with a stiffness of k<sub>c</sub> is added at the lower node of the insulator string. To accurately model the boundary conditions and analyze the effects of adjacent spans on the stiffness of the tower of interest, three different finite-element models representing 3, 5, and 7 tower-conductor systems were created, and nonlinear static pushover analysis was carried out for the three systems in the longitudinal and transverse directions. Once the curves had been obtained, each of the individual systems were reduced to their corresponding equivalent models. Each consisting of a single tower of interest with conductor spans present on both sides and equivalent springs

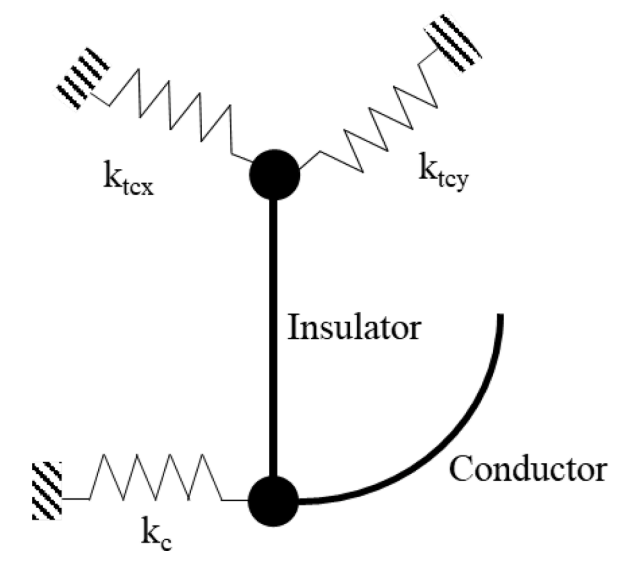


Fig. 3. Simplified boundary conditions.

added at the boundaries to simulate the effect of additional spans present in the original system. Fig. 4 shows the different finite-element configurations tested. The stiffness  $k_c$  added at the boundary conditions for each of the configurations have an analytical form of the stiffness for the conductors due to (Veletsos and Darbre 1983):

$$k_c = \frac{1}{1+\rho} \frac{AE}{L_e} \cos^2 \theta + \frac{T_o}{L} \sin^2 \theta \tag{1}$$

$$\rho = \frac{1}{12} \frac{AE}{\sin L_e} \left( \frac{q_y L}{T_o} \right)^2 \tag{2}$$

where A and E are the cross-sectional area and the elastic modulus of the transmission conductor, respectively;  $\theta$  is the inclination of conductor;  $T_o$  is the conductor tension;  $L_e$  is the effective conductor length equal to  $L \times [1+8 \times (\text{sagging}/L)^2]$ ; L is the distance between the two suspension points of the transmission conductor; and  $q_y$  is the intensity of normal load per unit of conductor length.

Fig. 4 shows the tower with a dotted circle representing the tower of interest and adjacent towers replaced with elastic springs representing the elastic stiffness of the tower of interest obtained from the pushover curve for the original configurations. The conductors are replaced by springs representing the conductor stiffnesses obtained from Eq. (1). Fig. 4 shows the results obtained for the pushover analysis in the transverse direction for the tower of interest for both a full model of adjacent towers and equivalent model of adjacent towers.

Based on the results in Fig. 4, it can be seen that by adding springs that simulate the stiffness of additional spans, including the conductors and towers, a good approximation for the structural behavior of the tower of interest was achieved with simulation of 5 and 7-tower systems. Therefore, the equivalent model with five towers was considered for its computational efficiency.

#### 3. Uncertainties, failure modes, and limit states

#### 3.1. Treating the uncertainty in structural parameters

When considering uncertainty in structural parameters, since a deterministic finite-element model cannot be used to conduct an uncertainty analysis for the transmission tower system, it is important to establish uncertain finite-element models. The uncertainty analysis procedure adopted for this study is shown in Fig. 5. The primary task of uncertainty analysis is to select the uncertainty variables and determine their corresponding probability distributions. For a transmission tower,

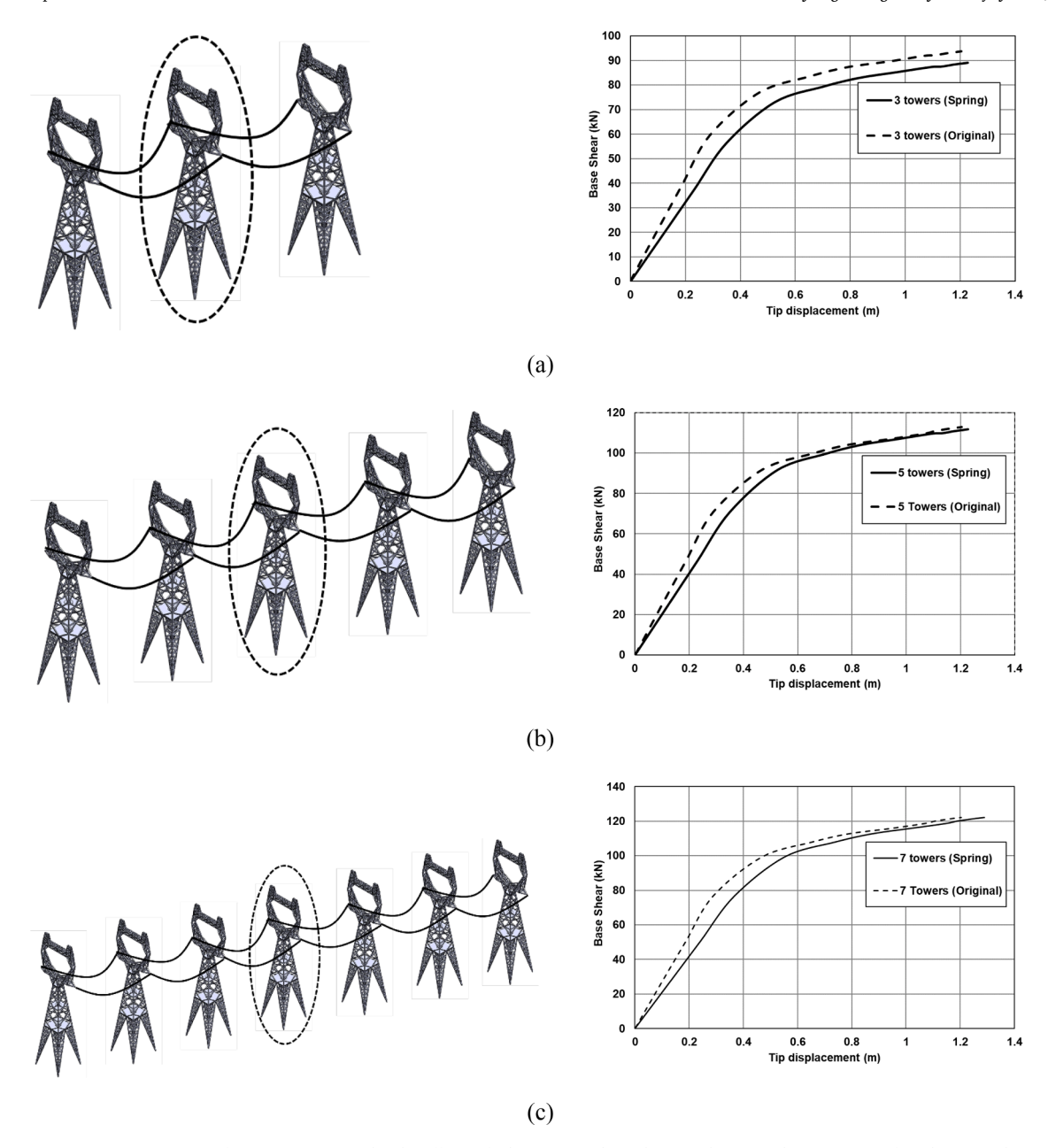


Fig. 4. Different transmission system configurations to consider the effects of adjacent span boundary conditions and comparison of nonlinear pushover analysis: (a) 3 towers; (b) 5 towers; (c) 7 towers.

there are a number of random variables, and it is important to consider them properly in the analysis.

A number of uncertainty structural parameters exist in any structure, including geometric dimensions, material properties, and boundary conditions. Variability in any of these parameters can lead to uncertainty in the structural resistance. In this study, the boundary conditions are clearly defined for the simplified transmission tower. The legs of the tower of interest are fixed supports and the end of the conductors on either side of the tower have springs present to account for stiffness from additional spans, so the material properties and geometric dimensions are selected as the random variables to generate the random samples for establishing the uncertainty finite-element models for the transmission tower. Most of the tower materials are constructed from steel whose main properties are density, elastic modulus, Poisson's ratio, and yield strength. Table 5 lists the probability distributions of the material variables considered [46].

Once the underlying probability distributions for the material

properties are determined, it is important to select samples from these distributions that can be used for establishing uncertain finite-element models. Traditionally, random samples are generated based on the technique of Latin Hypercube Sampling (LHS) [47], a selective sampling technique by which, for a desirable accuracy level, the sample size is significantly smaller than for direct Monte Carlo simulation [48]. To generate the uncertain finite-element models, the approach still requires multiple numbers of samples from each underlying distribution for the material properties. For example, the work done by Fu and Li [29], found that a sample size of 100 offered an adequate accuracy level. Since the present study aims to characterize the dynamic interaction and requires conducting dynamic wind analysis for each uncertain finite-element model, a very high number of dynamic simulations would be needed to capture structural uncertainty and randomness of wind loading, so in order to reduce the number of analysis steps required to produce reliable results for the fragility analysis, the efficient statistical method of moment matching (MM) was introduced. MM is a method of

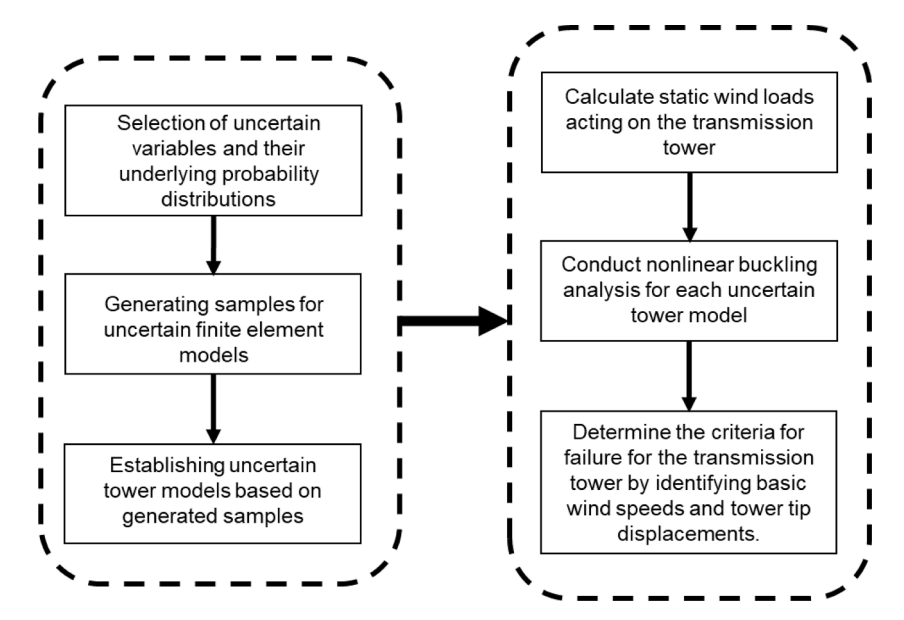


Fig. 5. Flowchart for considering structural uncertainty in transmission tower.

**Table 5**Probability distribution of material characteristics (adopted from [46]).

Uncertainty source	Average value	COV	Distribution type
Elastic modulus Density	200 GPa 7800 kg/m <sup>3</sup>	0.03	Lognormal Deterministic
Yield Strength	250 MPa	0.07	Lognormal

representing a large population with a substantially smaller sample size while preserving statistical moments (e.g., mean, variance, skewness, kurtosis, etc.). MM's sample size is an order of magnitude smaller than that of other random sampling methods such as Monte Carlo Simulation and the Mean and Sigma method. The methodology is used in the seismic risk assessment but is not explored for wind-risk assessment. For example, a study by Cho and Porter [49] on large-scale earthquake-risk assessment examined the difference between the moments of the sample and surveyed population (i.e., error) using the MM and Mean and Sigma methods. The results showed that in the Mean and Sigma method the error in calculating the first moment of the sample E[x] was 1.62%, and for the higher moments up to  $E[x^5]$ , the error increased to as much as 28%. However, for the MM method, the maximum error for  $E[x^5]$  was found to be 0.005% for the same variable. This indicates that the MM method error is reliable only for calculating mean value for a symmetric and regular form of data and performs poorly in estimation of higher-order moments for each predictor/variable. In this study, each of the selected uncertain material variables have an underlying probability distribution function (PDF). Using the MM technique, the next step is to generate a discrete probability function that can statistically represent a continuous PDF for each of the selected variables in the study. This discrete probability can be considered as a probability mass function (PMF) consisting of positions and their associated weights for each variable. In this study, as recommended in Cho and Porter [49], to avoid computational complications, the PMF for each variable consists of three positions and their associated weights. The weights and positions of the PMF are chosen such that first five moments (mean, variance, skewness, etc.) of both the discrete PMF and the original PDF are identical [50]. Detailed procedures outlining how the three positions and their weights for each studied variable are calculated such that the resulted PMF exactly match the first five moments of variable's distribution are given in the work done by Cho and Porter [49]. The next step combines all PMFs and develops a junction distribution of all the variables' PMF. This results in 2n + 1 index values, where n is the number of selected

variables considering material uncertainty in this study. In this study, there are two key variables representing material uncertainty: Young's modulus and yield stress. This results in five index positions or five sets of the two selected material parameters, i.e., each position corresponds to a set having a given Young's modulus and yield stress value. Also, each of those index values have their own associated weights. Considering each material variable as an axis with three positions and their associated weights, combining 2 axes would result in a 2-dimensional junction distribution. Since all these axes share one of their three positions to make the centroid of the 2-dimensional junction distribution, the final number of positions in the 2-dimensional junction distribution would be 2 multiplied by 2 plus 1, which results in 5 index material parameter values. These five index material parameter values can be used to set up five uncertain finite-element models, each having its own weight. The weight for the center of these axis  $w_1$  can be obtained using Eq. (3) shown below:

$$w_i = 1 - \sum_{i=1}^{2n+1} w_i \tag{3}$$

where n is the number of variables and  $w_i$  is the associated weight of each index finite-element model

For variables with a predefined underlying probability distribution, it is a trivial task to select samples and assign weights (importance factors) to each of the selected samples. For variables where the underlying distribution is not clear, a numerical moment-matching method (NMM) can be employed. Table 6 lists the selected sample values and weights for each of the uncertain material variables. Once the sample values and associated weights for each of the uncertain variables are determined, combinations of the resultant samples are generated with their associated weights that are then used to establish the uncertain finite-element models. It can be seen that only five uncertain finiteelement models need to be established to account for uncertainty in structural parameters. Based on work done by Fu et al. [44], it was found that to include material uncertainty based just on yield strength, the number of selected samples or uncertain finite-element models based on LHS were 20. If another variable representing material uncertainty was added, the number of required samples would have increased by  $20^2$ , a significantly higher number than the number of samples generated using the MM technique as in this study, hence enhancing the computational efficiency of the proposed method. Table 7 shows the list of uncertain finite-element models along with their associated material properties.

Table 6
Selected samples for uncertain finite element models from MM.

Uncertainty source	Sample 1 (S <sub>1</sub> )	Weight for S <sub>1</sub>	Sample 2 (S <sub>2)</sub>	Weight for S <sub>2</sub>	Sample 3 (S <sub>3</sub> )	Weight for S <sub>3</sub>
Elastic modulus (GPa)	189.79		200.00		210.56	_
Viold atmomath (MDa)	220.94	0.16	250.00	0.67	281.49	0.16
Yield strength (MPa)	220.94	0.16	250.00	0.67	281.49	0.16

**Table 7**Number of uncertain finite element models with MM.

Index value/uncertainty source	Elastic modulus	Yield strength	Weight
1	200 GPa	250 MPa	0.36
2	189.79 GPa	250 MPa	0.16
3	210.56 GPa	250 MPa	0.16
4	200 GPa	220.94 MPa	0.16
5	200 GPa	281.49 MPa	0.16

# 3.2. Failure modes and limit states for transmission tower, conductors and insulators

An explicit form of the limit states is not available for a complex system such as the tower-cable system. Many different techniques have been used to determine empirical forms of the performance functions (limit state curves) that can assist in assessing the vulnerability of the transmission tower in response to wind loads. [51] used statistical learning theory and machine-learning algorithms to predict the failure surfaces for the transmission towers. Sandage [52] used regression analysis based on numerous numerical simulations for a finite-element model of a transmission tower to generate empirical forms of the performance functions for transmission towers subjected to wind loads and unbalanced ice loads. Fu, Li, & Li [26] used the critical-collapse curve concept for transmission towers subjected to wind and rain loads by gathering the collapse equivalent basic wind speed and generating sets of the most unfavorable combinations of wind and rain loads.

For the transmission tower, the immediate cause of tower collapse is not a loss of material strength but rather member buckling due to the presence of initial eccentricity [26] that is inevitable during the structural construction process. The initial uniform mode method that assumes that the distribution of initial eccentricity is consistent with the lowest buckling mode, has been widely accepted in evaluating the influence of initial eccentricity on structural stability. In this study, the initial uniform mode method was employed to conduct the nonlinear static analysis of a transmission tower. The relatively complex underlying buckling analysis involves evaluation of a previous static solution while including pre-stress effects. The flowchart of Fig. 6 represents the ANSYS process of non-linear buckling analysis subjected to a wind load. It is of utmost importance to notice that only the lowest buckling mode is used to update the geometry of the FEM. Euler elastic buckling analysis is carried out in ANSYS to obtain the lowest buckling mode used to introduce initial imperfection/eccentricity into the structure. A nonlinear static analysis is then carried out for the structure where static wind loads considering material and geometric nonlinearities are applied. The buckling point is identified as a point where the structure begins exhibiting large deformations with incremental increases in wind loads. Fig. 7 shows the buckling analysis results when the wind loads are applied along the longitudinal direction of the transmission tower. In a similar fashion, for each of the uncertain finite-element models, buckling analysis was carried out for wind loads while also considering different wind directions. This resulted in limit states for buckling for each of the uncertain finite-element models for all the considered wind directions. The results obtained for the tip displacement for different directions are shown in Table 8.

Another limit state that can be identified for the transmission tower is yielding of the material used in tower construction. The post buckling

behavior of the transmission tower was studied after establishing the buckling point. It can be seen in Fig. 7 that, once the buckling point was established, the steel material that was used for constructing the tower members had not yet yielded. For understanding the post buckling effect, with an increase in static wind loads, it can be seen that at a displacement of 2.2 m, the tower material used for constructing began to yield, so it can be seen that transmission tower buckling is the dominant failure mode because it occurs before the actual yielding of the material sets in. This infers that, with the application of static wind loads after the buckling point, the tower continued to deform until the material also vielded. In a similar fashion, for each of the uncertain finite element models, post-buckling behavior was studied for wind loads while also considering different wind directions. This resulted in limit states for yielding for each of the uncertain finite-element models for all the considered wind directions. The results obtained for one of the uncertain finite element models are depicted in Fig. 8, showing the different stages observed during the complete analysis of determining the buckling point and yielding point for the tower when the wind loads are acting in the longitudinal direction.

Since the insulators and conductors presented in the study were the simple truss members defined in Section 2.1, the only failure mode that could be identified was axial stress of the truss members comprising the conductor or the insulator exceeding the defined yield stress of the material used for modeling the conductors and insulators, respectively.

#### 4. Wind load

Wind speed and direction vary both spatially and temporally. Due to the inherent dynamic nature of wind, the wind load is a key design load for structures, especially for transmission tower systems. Generally, wind tunnel tests, field measurements, or numerical simulations determine design wind loads, and currently, numerical simulation of wind is widely-used and trusted in civil engineering. One important aspect introduced in this paper is the coherence function for the wind loads, which is not only considered in the vertical direction along the height of the tower but also along the horizontal direction, and including the conductors connected to the tower. Variations in both vertical and horizontal directions provide a realistic behavior of the tower-cable system and help in developing accurate fragility curves. The approach utilized in this paper for the vertical variation of the wind loads involves using a Kaimal fluctuating wind-power spectrum and a harmonic superposition method to simulate the stationary stochastic processes [53]. For simulating the variation of the wind loads along the horizontal direction, including the cable, the frequency wave spectrum method proposed by Benowitz & Deodatis, [54] has been adopted.

#### 4.1. Wind conditions

The total wind velocity in any point of a structure is the sum of the mean wind velocity and the turbulent wind velocity:

$$v(z,t) = \overline{v}(z) + v_t(z,t) \tag{4}$$

where v(z,t) is the total wind velocity acting on the structure,  $\overline{v}(z)$  is the mean wind velocity, and  $v_t(z,t)$  is the turbulent wind velocity.

The mean wind component of the total velocity is often expressed by a logarithmic or exponential function associated with the height; this is known as the log law of the variation of wind velocity with height:

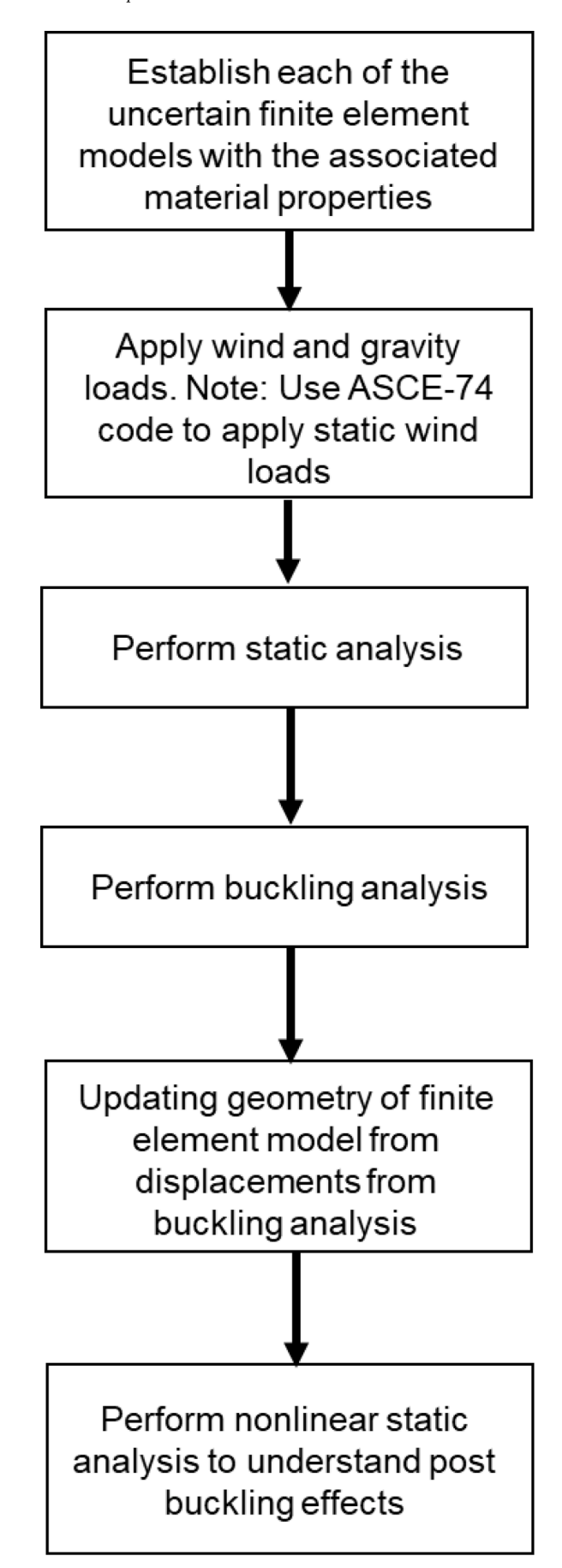


Fig. 6. Flowchart for performing buckling analysis for wind loads.

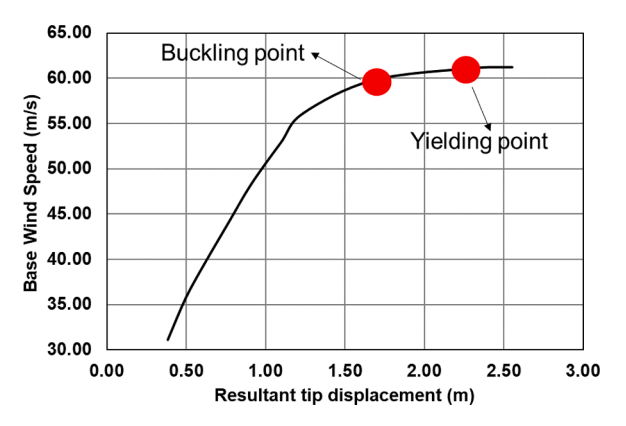


Fig. 7. Buckling analysis for uncertain finite element model (Index 1).

**Table 8**Resultant tip displacement for nonlinear buckling analysis.

Wind direction (degrees)	Resultant tip displacement (m)
0	1.72
15	1.64
30	1.58
45	1.84
60	1.67
75	1.86
90	2.14

$$\overline{v}(z) = \frac{1}{k} u_* \ln \frac{z}{z_0} \tag{5}$$

where k is the Karman constant equal to 0.4,  $\overline{\nu}(z)$  is the mean wind speed of z, z is the standard height,  $z_o$  is the ground roughness length (m), and u\* is friction velocity.

The fluctuating wind can be visualized as a 3D turbulent flow made up of three components: along-wind, across wind, and vertical-wind, and the power spectrum in all the three directions can be used to describe the fluctuating behavior in the three directions. According to the characteristics of a transmission tower-line system, only the along-wind dynamic response is considered in this study, and the along-wind Kaimal fluctuating wind power spectrum is given by Eq. (6).

$$\frac{nS(f)}{u_*^2} = \frac{200x}{(1+50x)^{3/2}} \tag{6}$$

where x is the nz/V(z) is the dimensionless coordinate, z is the height of the simulation point, f is the frequency of fluctuating wind, and  $u^*$  is the friction velocity.

#### 4.2. Wave superposition method

The harmonic superposition method is a discrete numerical method for simulating a steady random process. This method is useful because the signal can be considered to consist of a sum of a series of sinusoidal waves with different frequencies and amplitudes that can be extracted using the Fourier transform. The turbulent part of the wind, essentially a random process, can be described by its power spectrum. When  $N \to \infty$ , using the theory presented by Shinozuka & Jan [55], the fluctuating wind velocity time series  $u_i(t)$  is satisfied by Eq. (7).

$$u_{i}(t) = \sum_{l=1}^{i} \sum_{k=1}^{N} |H_{il}(\omega_{k})| \sqrt{2\Delta\omega_{k}} \cos[\omega_{k}t - \theta_{il}(\omega_{k}) + \varphi_{il}] i = 1, 2, ...m$$
 (7)

where N represents the division numbers of fluctuating wind frequency, i refers to the calculation point numbers,  $H_{ij}$  is obtained from Cholesky decomposition of the wind cross-spectral density matrix,  $\theta_{il}(\omega)$  is the

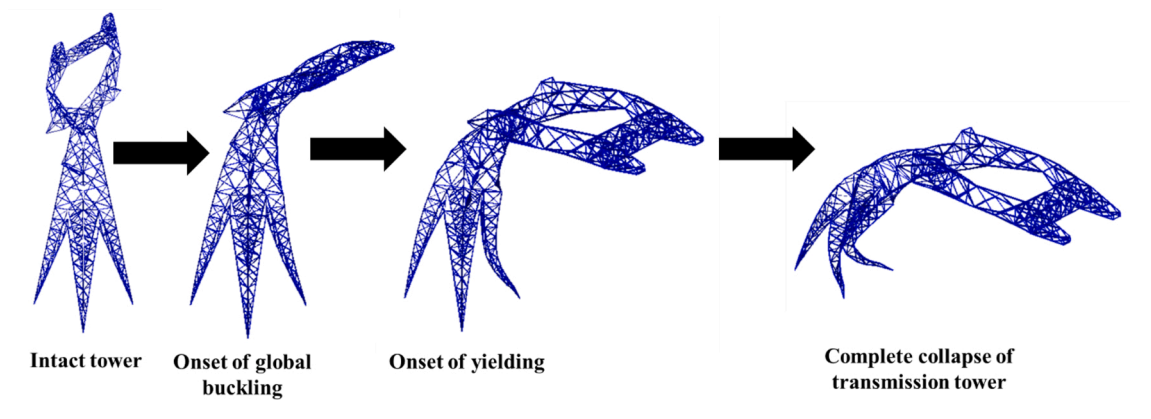


Fig. 8. Buckling analysis for the transmission tower model along longitudinal direction.

argument of  $H(\omega)$ ,  $\varphi_{il}$  denotes the uniformly-distributed random numbers in  $[0, 2\pi]$ , and  $\omega_u$  is the upper limit circle frequencies of fluctuating wind as follows:

$$\int_{0}^{\omega_{n}} S(\omega)d\omega = (1 - \varepsilon) \int_{0}^{\infty} S(\omega)d\omega$$
 (8)

where  $(\omega)$  is the autopower spectrum density function, much smaller than 1,  $\Delta\omega_k$  is a frequency increment, and  $\Delta\omega=(\omega_u-\omega_s)/N$ . To increase the period of the simulated sample, Shinozuka and Deodatis [53] suggested that:

$$\omega_k = k\Delta\omega_k - \frac{N-l}{N}\Delta\omega_k = (k-1)\Delta\omega_k + \frac{l}{N}\Delta\omega_k \tag{9}$$

Positive integer N should be defined as sufficiently large to avoid the result of distortion in Eq. (4); the number of samples in the simulated time series should be more than 2 N, and the time increment should be small enough ( $\Delta t \leq \pi/\omega_u$ ). Therefore, the time increment must be considered as follows:

$$\Delta t = \frac{T_0}{M} = \frac{2\pi}{M\Delta\omega} = \frac{2N}{M} * \frac{\pi}{\omega_u}$$
 (10)

where M is an integer and  $M>2\,$  N. Based on the aforementioned technique, the wind time histories with the fluctuating component can be generated.

#### 4.3. Frequency-wavenumber spectrum method

For simulation of the wind time histories along the horizontal span of the cable, the methodology suggested by Deoditas [56] was utilized. In this approach, a virtually infinite number of spatial points can be simulated precisely by treating wind velocities as a continuous 'wave' in space–time rather than a discrete vector in space and continuous only in time. Sample generation is eased by using the Fast Fourier Transform (FFT) to achieve efficiency and reduce computation time. A frequency wave number spectrum number continuous in both time and space is suggested to enable modeling of an infinite number of wind velocities along the span of the cable. The relationship between the cross-spectral density matrix or auto spectrum and the coherence function can be converted into the frequency wavenumber spectrum using the following approach. It is shown below that:

$$S(\omega,\kappa) = \frac{1}{2\pi} \int_{-\infty}^{\infty} S(\omega) \gamma(\xi,\omega) e^{i\kappa\xi} d\xi$$
 (11)

where  $S(\omega)$  is the auto-spectrum,  $\gamma(\xi,\omega)$  is the coherence model,  $\xi$  is the spatial separation distance,  $\omega$  is the angular frequency, and  $\kappa$  is the wavenumber

The Kaimal spectrum has again been used in the formulation. Davenport's coherence function is adopted as the coherence function given by:

$$\gamma(\xi,\omega) = e^{-\lambda\omega\xi/2\pi U(z)} \tag{12}$$

where  $\lambda$  is a decay parameter, often chosen to be between 7 and 10.

Combining the above two equations, by using the Kaimal spectrum and the Davenport coherence function, the frequency-wavenumber spectrum can be shown to be:

$$S(\omega,\kappa) = \frac{1}{2} \frac{200}{2\pi} u_*^2 \frac{z}{U(z)} \frac{1}{\left[1 + 50 \frac{\omega_z}{2\pi U(z)}\right]^{53}} \frac{1}{2\pi} \int_{-\infty}^{\infty} e^{-\lambda \omega_\xi^2/2\pi U(z)} e^{i\kappa\xi} d\xi$$
 (13)

The Fourier integral in the above equation has an analytical solution given by Haberman [57] that changes the above expression to:

$$S(\omega,\kappa) = \frac{1}{2} \frac{200}{2\pi} u_*^2 \frac{z}{U(z)} \frac{1}{\left[1 + 50 \frac{\omega z}{2\pi U(z)}\right]^{53}} \frac{\frac{\lambda \omega}{\pi U(z)}}{\kappa^2 + \left(\frac{\lambda \omega}{2\pi U(z)}\right)^2}$$
(14)

Eq. (14) can be considered as a generalized closed form solution for generating wind velocities with spatial and temporal variations as a stochastic wave.

A variation of the spectral representation method (SRM) is used to generate sample realizations for a stochastic wave, as discussed in Section 4.2. The variation introduced in the expression is shown below:

$$u(x,t) = \sqrt{2} \sum_{l=1}^{N_k} \sum_{m=1}^{N_{\omega}} \sum_{I_{\omega}=\pm 1} \sqrt{2S_f(I_{\omega}\omega_m, \kappa_l)\Delta\omega\Delta\kappa} \cos\left[I_{\omega}\omega_m t + \kappa_l x + \Phi_{ml}^{I_{\omega}}\right]$$
(15)

The horizontal coherence functions are also shown for some of the locations in Fig. 9 to emphasize the importance of considering coherence along both the tower height and cable spans.

Once the time histories for the wind velocities are generated, the forces acting on the transmission tower system can be calculated.

#### 4.4. Applying wind loads to individual components

The wind loads/drag forces acting on each of the individual components including the tower, conductors and insulators are calculated using a variation of the standard formula for drag force calculation as shown below:

$$F(z,t) = 0.5\rho C_D v(z,t)^2 A$$
(16)

where, A is the projected area perpendicular to wind direction flow,  $C_D$  is the drag coefficient for each of the components, i.e., the tower, insulators, and conductors,  $\rho$  is the air density and v(z,t) are the time history of velocities that are generated for the tower, conductors and

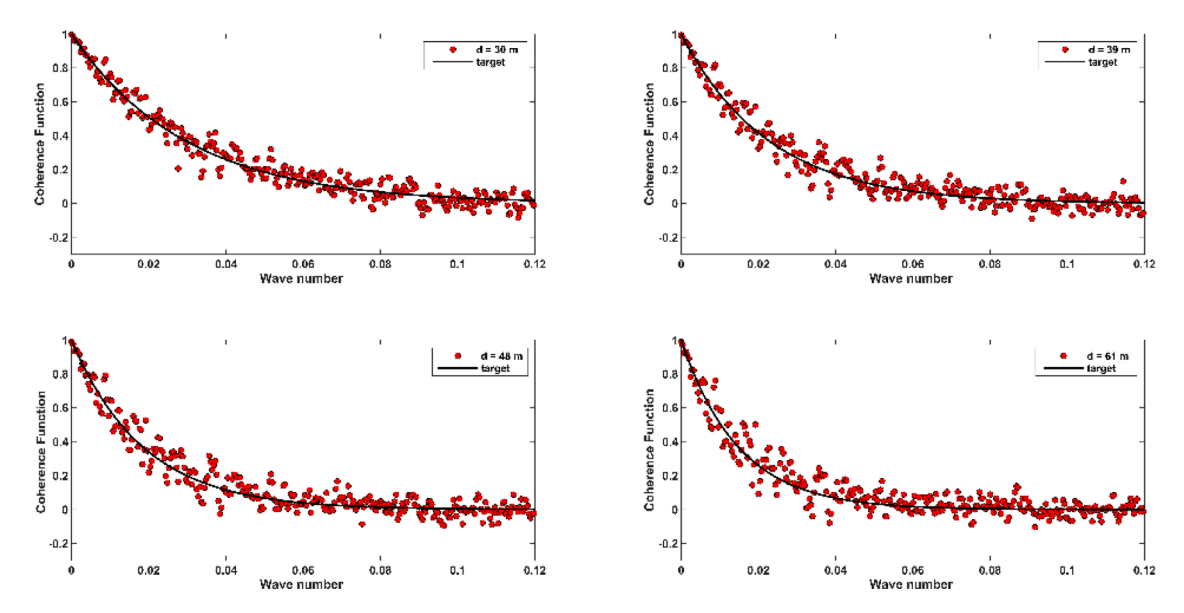


Fig. 9. Horizontal coherence function for 4 different locations along cable span.

insulators respectively as a function of time and height.

ASCE [9] utilizes the solidity ratio approach to calculate the drag coefficients acting on the transmission tower. This approach is conservative in nature and leads to overestimation of drag forces as mentioned in work done by Alipour et al. [40]. Thus, in order to generate realistic drag forces for the tower for different orientations, wind tunnel tests were carried out to obtain the drag coefficients for the tower by dividing the tower into three segments: the bottom part (legs), the middle part, and the top part. More information about how the drag coefficients were calculated for different tower orientations can be found in the work done by Alipour et al. [40].

The drag coefficients for the conductors based on ASCE [9] recommended using a value of 1 for calculation of drag forces. This value could again be conservative and unrealistic in nature. Thus, realistic drag coefficients for conductors based on work done by Jafari & Sarkar [41] for different wind directions were utilized for calculation of drag forces acting on the conductors. For the insulators, not much information was available. Thus, a recommended value of 1.2 based on IEC [11] was

utilized as the drag coefficient for the insulators. Once the drag coefficients for each of the components were determined, the wind loads were calculated at centroid locations for the components. For example, since the tower was divided into three sections, three separate centroid locations corresponding to the individual parts (top, middle and bottom) of the tower were used to apply the wind loads. Similarly, the conductors were divided into 100 segments and the wind loads were calculated for each of the centroid locations for each of the segments composing the conductor. The insulator string consisted of a single element and the wind load was calculated at the centroid of this segment.

Fig. 10 is a schematic of the loading pattern applied to the transmission tower system considering the tower along with the cables. Fig. 11 depicts the procedure for calculating the dynamic wind loads acting on each of the components of the transmission tower system including vertical coherence along the height of the tower and horizontal coherence along the span of the conductors.

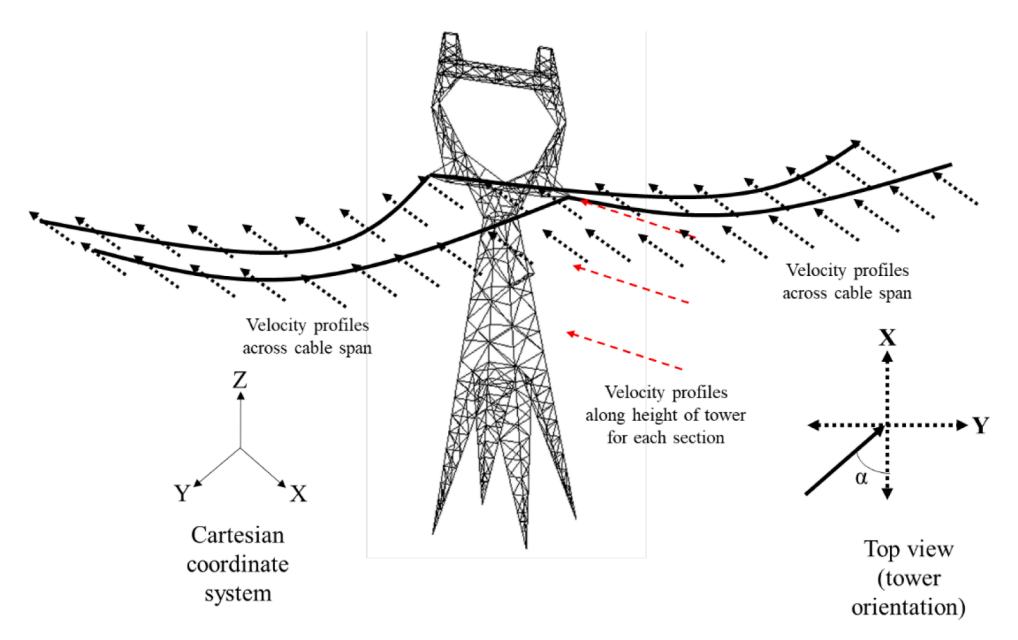


Fig. 10. Schematic for loading pattern for the transmission tower system considering the loads on the tower and the cables.

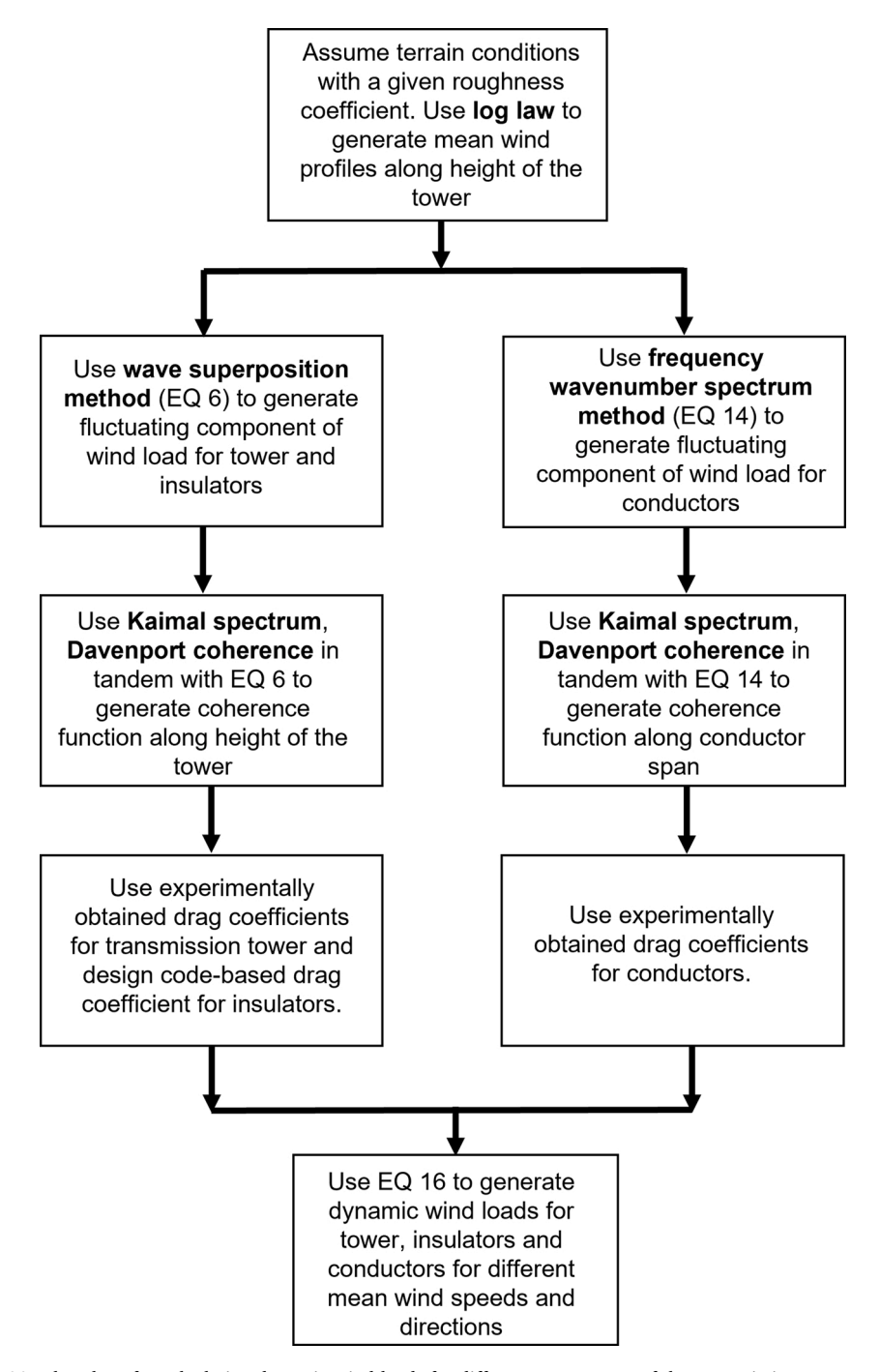


Fig. 11. Flowchart for calculating dynamic wind loads for different components of the transmission tower system.

#### 4.5. Dynamic wind analysis

A dynamic wind analysis of the tower system was carried out, with mean wind speeds ranging from 0 to  $100 \, \text{m/s}$  (intervals of 5 m/s) at a 10 m height applied to the model. The transient wind loading was applied for a total of one hour. The wind load was applied along different directions of the tower cable system to seek understanding of the impact of wind direction on the fragility analysis. Time histories for the tip displacement in all the three directions for the tower along with the axial stresses in the cable and insulator elements were recorded at each of these speeds. Failure of the system was considered to occur under three possible conditions:

- 1 the axial stresses in the cable elements exceeding their yield stress, leading to the failure of the cables, resulting in loss of utility of the transmission system
- 2 the axial stresses in the insulator elements exceeding their yield stress, leading to the failure of the insulator, resulting in loss of connection between the tower and the conductors
- 3 the tip displacement of the tower exceeding limit states established during the nonlinear pushover analysis, leading to failure of the tower in the transmission system.

Thus, failure for the complete transmission tower system was declared when any combination of the aforementioned conditions were met.

The simulation was carried out 100 times for each wind speed to

consider the probabilistic nature of the wind velocity fields. This allowed for consideration of inherent variability in failure for an intact tower cable system and a system with broken conductors. This process was repeated for each of the established uncertain models. The final failure probability was established using Eq. (17).

$$P_f = \sum_{i=1}^{5} W_i p_i \tag{17}$$

where  $P_f$  is the final failure probability for the transmission tower,  $W_i$  is the calculated weight for each uncertain finite element model i, and  $p_i$  is the associated probability of failure for the i<sup>th</sup> uncertain model

Fig. 12-a and 12-b show the results for one of the realizations of tip displacement for a 15 m/s and a 70 m/s wind speed. Fig. 12-a shows that for a wind speed of 5 m/s, the resultant tip displacement (vector combination of displacements along the X, Y and Z directions) does not exceed the established limit state, while for a wind speed of 70 m/s (Fig. 12-b), it is exceeded due to buckling. Similarly, for each wind speed, the tip displacement for the tower and the axial stresses for the cable were recorded. Fig. 12-c also shows the axial stress in the middle cable element for a wind speed of 70 m/s. It can be seen that since the axial stress is greater than the yield stress of the material used, the cable element can be considered yielded, leading to a mode of failure in the conductor. These data have been used to generate the fragility functions used in the next stage.

Once the final failure probabilities were established for the range of tested wind speeds for each of the wind directions, a maximum likelihood (MLE) approach was utilized to fit obtained failure probability values to the existing form of the fragility curves in the literature that follow a lognormal distribution [44,32,35]. The procedure is described by Eqs. (18), (19), and (20). The fragility of the transmission tower is approximated as a lognormal distribution of form:

$$P(F|WS = x) = \phi \left(\frac{lnx - \mu}{\beta}\right)$$
 (18)

$$P(F|WS = x_j)_{observed} = \frac{number\ of\ failures\ when\ WS = x_j}{Number\ of\ simulations}$$
 (19)

$$P(z_j \text{ failures in } n_j \text{ wind simulations}) = \binom{n_j}{z_j} p_j^{z_j} (1 - p_j)^{n_j - z_j}$$
 (20)

where P(F/WS) is the probability of failure/collapse for a given wind speed WS, described as a standard normal cumulative distribution  $\phi$  of the natural log of x over  $\mu$  (median IM that causes failure) all over  $\beta$  (dispersion of IM) and  $z_j$  is the number of failures observed out of  $n_j$  simulations

Using the maximum likelihood approach, estimators  $\hat{\mu}$  and  $\hat{\beta}$  were used to approximate the actual parameters of the lognormal distribution in Eq. (18) by maximizing the likelihood of producing the observed data from the conducted dynamic analysis of the system. The function is shown in Eqs. (21) and (22).

$$Likelihood = \prod_{j=1}^{m} {n_j \choose z_j} p_j^{z_j} (1 - p_j)^{n_j - z_j}$$
(21)

$$\{\widehat{\mu}, \ \widehat{\beta}\} = \max \prod_{i=1}^{m} \binom{n_j}{z_j} \phi \left(\frac{\ln x_j - \mu}{\beta}\right)^{z_j} \left(1 - \phi \left(\frac{\ln x_j - \mu}{\beta}\right)\right)^{n_j - z_j}$$
(22)

where m is the number of simulated wind speeds

#### 5. Fragility analysis of tower system

#### 5.1. Fragility curves for buckling

Dynamic analysis for the complete transmission tower system was

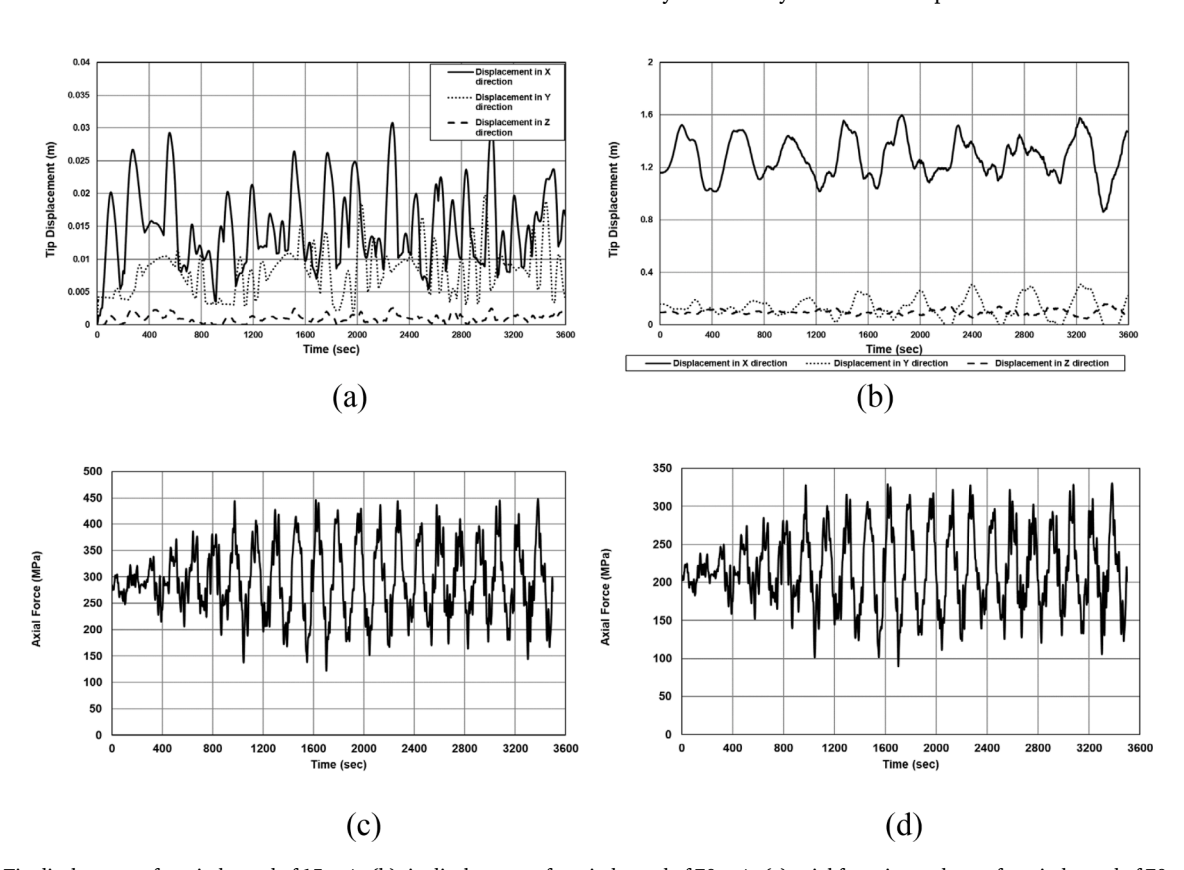


Fig. 12. (a) Tip displacement for wind speed of 15 m/s; (b) tip displacement for wind speed of 70 m/s; (c) axial force in conductor for wind speed of 70 m/s; (d) axial force in insulator for wind speed of 70 m/s.

carried out, with the tip displacement along the Cartesian coordinate system recorded for each of the simulations. Fig. 12-a shows the tip displacement results for 15 m/s and 70 m/s wind speeds. From Fig. 12-a, it can be seen that for a wind speed of 15 m/s, the resultant tip displacement (vector combination of displacements along the X, Y and Z directions) does not exceed the limit state established, while for a wind speed of 70 m/s, it can be seen that the resultant tip displacement exceeds the established limit state, reflecting a failure of inelastic buckling in the tower system. The established fragility curves for the failure mode of buckling for different wind speeds are shown in Fig. 13.

There is a narrow band of wind speeds where actual failure probabilities are observed. It can be seen that with increase in wind speed, the probability of failure of transmission tower system increases. At lower wind speeds (0 m/s to 45 m/s), for the majority of the simulations it can be seen that the tower remains intact, so the probability of failure is very low (close to zero). A noticeable aspect about the failure pattern that can be seen at medium range wind speeds (45 m/s to 75 m/s) is that in the majority of the simulations, the tower begins to buckle and is crossing the established limit state. Toward the higher end of the medium wind speed range, the tower begins to fail in a majority of simulations.

The process of obtaining fragility curves using the methodology established in the previous sections was repeated for wind loads applied to the transmission tower system at different angles or tower rotations. The wind loads are broken down into appropriate components along the transverse and longitudinal direction and applied to the tower cable system. Since the tower-line system has biaxial symmetry in both the x-and y-directions, only seven wind angles of attack with increments of  $15^{\circ}$  were considered. These were used to generate a set of seven fragility curves for the intact system. The generated fragility curves for different wind angles of attack for the intact transmission tower are also shown in Fig. 13. A large gap is visible between fragility curves for different angles of attack; with an increase in the angle of attack, the curve shifts to the right. At a  $60^{\circ}$  angle of attack, the curves shift to the left. Also, for each angle of attack, there is an associated limit state for buckling. This leads to the pattern observed in the fragility curves.

#### 5.2. Fragility curves for yielding

Dynamic analysis was carried out for the complete transmission tower system, and the established fragility curves for the failure mode of yielding for different wind speeds are shown in Fig. 14.

Again, a similar pattern is observed in the obtained fragility curves as

in the fragility curves of Fig. 13. One noticeable aspect is that the curves for different wind angles of attack have shifted to the right. This behavior is expected because the limit state for yielding of the transmission tower is higher than that of buckling. There is a narrow band of wind speeds where actual failure probabilities are observed. It can be seen that, with increases in wind speed, the probability of transmission tower system failure increases. At lower wind speeds (0 m/s to 55 m/s), for the majority of the simulations, it can be seen that the tower remains intact, i.e., the probability of failure is very low (close to zero). A noticeable aspect about the failure pattern that can be seen at mediumrange wind speeds 55 m/s to 80 m/s) is that in majority of the simulations, the tower begins yielding and crossing the established limit state. Towards the higher end of the medium wind speed range, the tower starts failing for a majority of simulations.

Fragility curves for the transmission tower were re-established for different angles of attack for the limit state of yielding. It can be seen from Figs. 13 and 14 that the wind attack angle has a major influence on the failure probability of the tower cable system, with a large gap visible between fragility curves for different angles of attack. With an increase in the angle of attack, the curve shifts to the right, and at an angle of attack of  $60^{\circ}$ , the curves shift to the left. A possible underlying reason for this curve behavior seen is related to the components of wind loads acting in the transverse and lateral directions, i.e., as the angle of attack increases, the transverse component decreases and the longitudinal component increases. Also, for each angle of attack, there is an associated limit state for buckling and yielding. This leads to the patterns observed in the fragility curves.

Another noticeable aspect observed for the fragility curves due to yielding is that the dominant failure mode for the transmission tower is due to buckling of the tower members, leading to instability in the transmission tower. The fragility curves observed for the same wind speeds and wind directions due to yielding are shifted to the right in comparison to the ones due to buckling. This is because the actual limit states for yielding are higher than that of buckling. The tower members buckle before actual material yielding in the members. Thus, of the two different failure modes, the fragility curves established for buckling are the more critical.

#### 5.3. Fragility curves for conductors and insulators

As discussed in Section 3.2, the failure of the conductors and insulators is assumed when the axial stresses in the members exceeds the

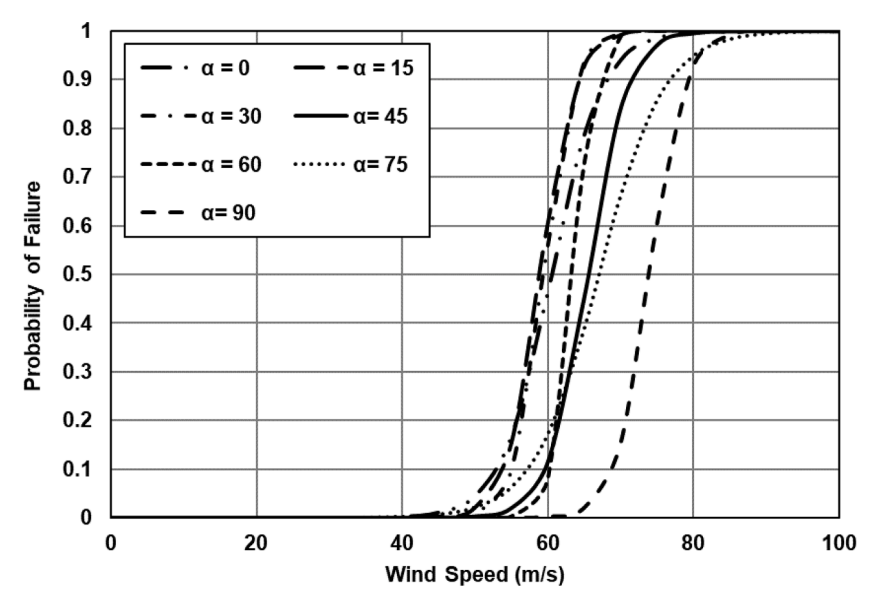


Fig. 13. Fragility curves for the intact transmission tower (failure mode buckling).

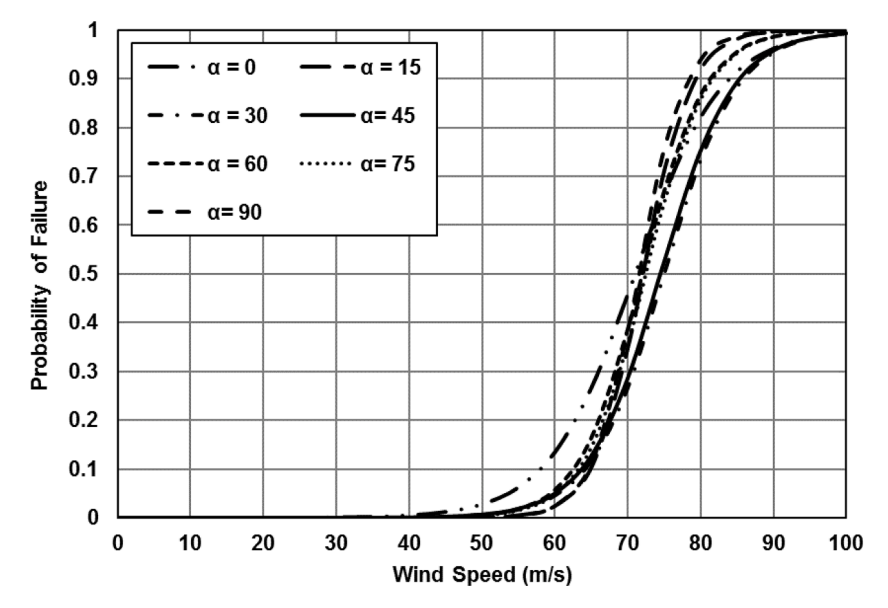


Fig. 14. Fragility curves for the intact transmission tower (failure mode yielding).

yield stress of the material used for constructing the components. Figs. 12-c and 12-d show the axial stresses in conductors and insulators for a wind speed of 70 m/s. It can be seen that the stresses exceed the yield stress of the material. The established fragility curves for the conductors and insulators for different wind speeds and wind angles of attack are shown in Figs. 15 and 16 respectively. The established fragility curves for both the components have a narrow band as well in which actual failures occur in these components. Based on work done by Jafari and Sarkar [41], the observed variation in fragility curves for different angles of attack for conductors and insulators is due to the difference in drag coefficients for conductors in different directions. Also, in the case of insulators, the difference in fragilities for different angles of attack is due to the difference in the projected area experienced by the insulators at different angles.

#### 5.4. Fragility curves for intact and damaged system

Based on the fragility curves established for each of the individual components associated with the transmission tower system, the fragility curves for the intact system can be obtained based on the failure criteria set in Section 4.5. The generated fragility curves for the intact system are presented in Fig. 17. Another state for the transmission tower system that includes damaged conductors was also established. This system state was created by extracting the force-time histories at the towerinsulator-conductor connection joint and applying them as additional time histories on the intact transmission tower using the element birth/ death approach in ANSYS explicit analysis. The ANSYS explicit analysis deletes the conductor element present at the tower conductor joint location and records the axial stresses occurring in the adjacent conductor elements. The time histories of additional axial stresses are then applied to the intact system, making the transmission tower more susceptible to failure due to this addition of the forces, and shifting the fragility curves to the lift, indicating that the system now fails at lower wind speeds. Also, from Fig. 17 it can be seen that the systems with broken conductor/cables have higher probabilities of failure compared with the one with the intact system. This can be attributed to the fact that the system with the broken conductors has unbalanced loads that are not being transferred to the tower through the pin connection joints.

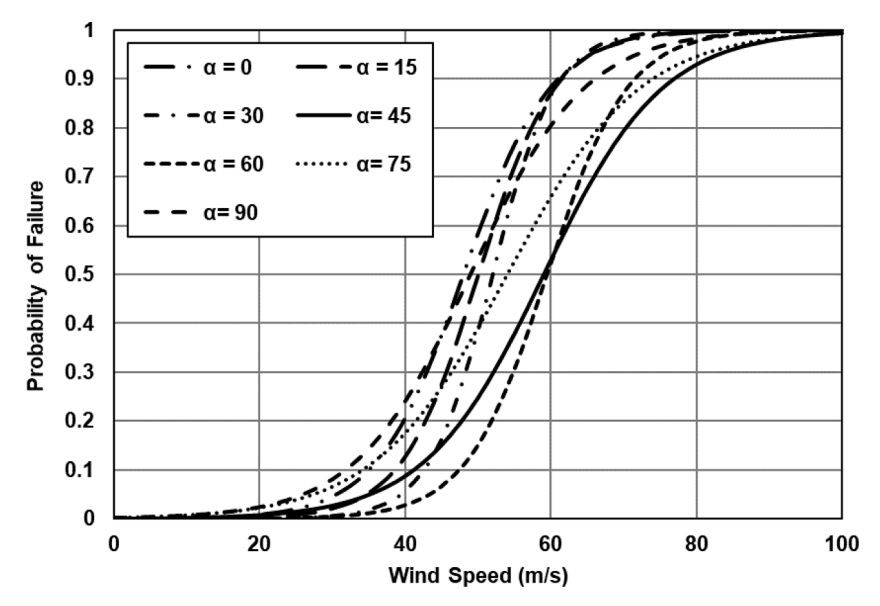


Fig. 15. Fragility curves for the intact conductors.

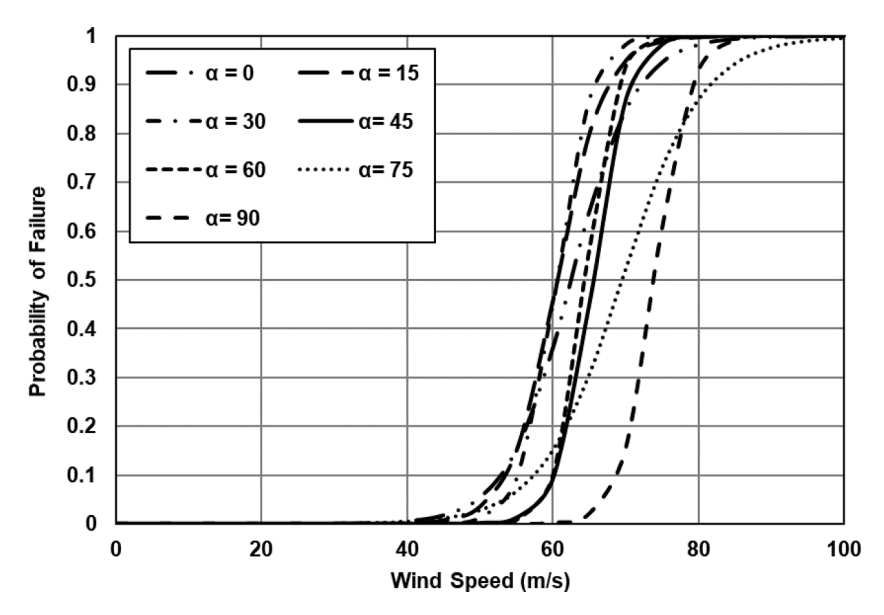


Fig. 16. Fragility curves for the intact insulators.

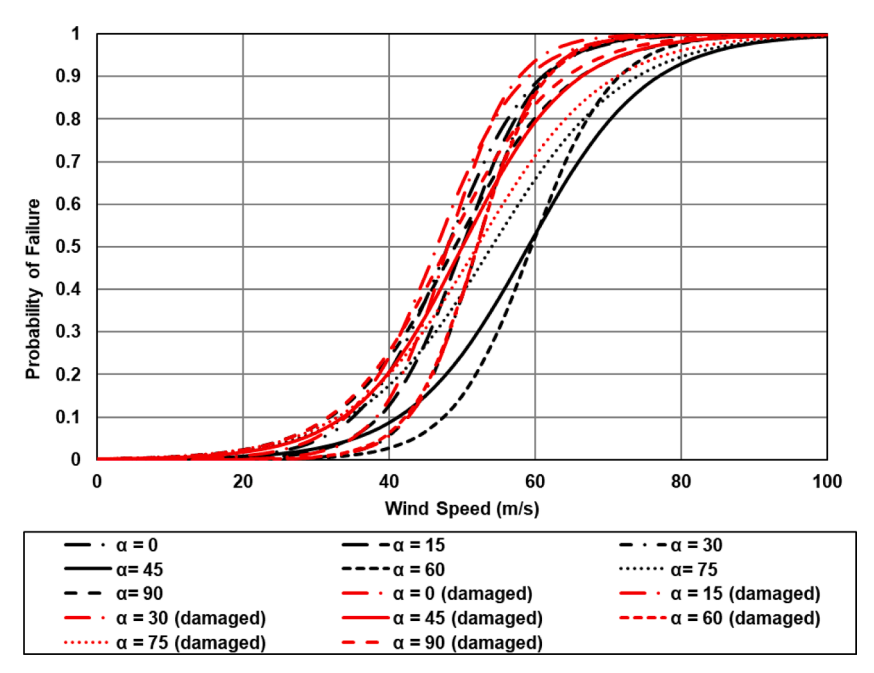


Fig. 17. Fragility curves for intact and damaged system.

Thus, at a given wind speed, with the added wind loads, the tower cable system fails earlier than the intact system.

#### 5.5. Comparison of fragility curves employing MM and LHS

It is to be noted that the fragility curves generated in all the preceding sections employ the MM technique to significantly reduce the computational time required. To understand the implications of this approach compared to the conventional LHS approach, fragility curves were generated for a given tower orientation using the LHS approach. The results obtained are shown in Fig. 18. It can be seen that the obtained fragility curves using the MM approach are very similar to the ones obtained from LHS approach. This reiterates the strong impact of MM versus LHS in which the computational time is drastically reduced with a reduction in the number of required samples using MM while maintaining the accuracy of results observed using a conventional LHS

approach.

### 6. Conclusions

A probabilistic approach has been presented for assessing the vulnerability of transmission tower systems to dynamic wind loadings. The proposed framework properly addresses uncertainties originating from applied wind loads and uncertainties arising from material properties. However, numerous simplifications were made when deriving the fragility curves.

For example, joints are semirigid in reality, while ideal rigid or pin joints are adopted in the finite-element model presented in this study. It is also assumed that the tower legs are constrained rigidly by the foundation, so that the effects of soil –structure interactions can be neglected. These issues are of practical importance and should be addressed in future studies. To ensure that the fragility analysis could be

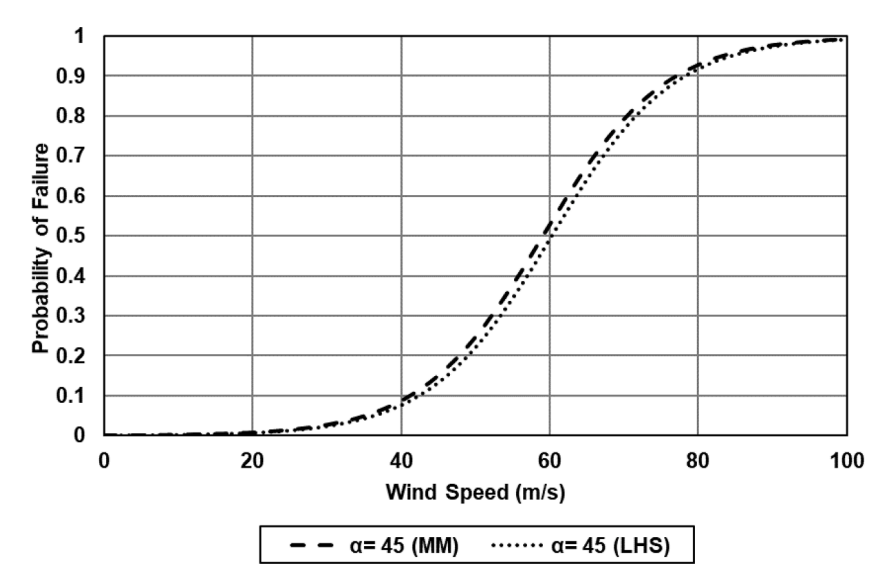


Fig. 18. Comparison of fragility curves (MM vs LHS).

performed within an acceptable computational time, a simplified model with one tower and two span lines was presented and validated via a comparison with a complete tower-line system under both static conditions. A real operational transmission line was employed in this study. The wind speed and direction are not independent; they exhibit a coupling effect, so this paper separately discusses the influence of wind direction on a fragility curve and does not consider the joint influence of wind speed and wind direction. In the future, a joint probability distribution model of wind speed and direction can be fitted via measured meteorological data to further assess the probability of failure and the wind-resistance performance of transmission towers under wind loads. While most transmission towers collapse during nonstationary typhoons or hurricanes, the characteristics of nonstationary winds and the induced structural responses are different from those of stationary winds, so in the future a nonstationary wind can be considered in fragility analysis.

Capacity curves for the transmission tower were established to compensate for the lack of explicit forms of the performance functions for the tower. Limit states were established based on the capacity curves. Nonlinear dynamic analysis was carried out for the tower cable system to assess the effects of dynamic wind loads. Uncertain finite-element models considering material variability were established. A momentmatching method was utilized to select the samples used for establishing these uncertain finite element models. With the established uncertain finite-element models, dynamic analysis was carried out for each of these models to consider uncertainty in wind loadings.

Variations of wind load both in the space domain (vertical and horizontal) and the time domain were considered. Fragility curves were established for the tower cable system for two particular conditions, i.e., an intact tower cable system and a tower system with broken conductors. These fragility curves help in understanding the probabilistic nature of failure of these tower cable systems in response to wind loadings. This can lead to better design of such tower cable systems which are reliable in nature and less susceptible to failure due to wind loads. The presented fragility framework can be used to develop performancebased design guidelines for transmission towers in high-wind regions as well as to provide information on structural safety and expected structural or economic loss assessments [58]. The proposed fragility analysis also offers a way to estimate the probability of failure under different wind speeds. Accordingly, either the probability of failure or the reliability index can be easily calculated using meteorological data recorded nearby [29].

#### CRediT authorship contribution statement

**Saransh Dikshit:** Data curation, Formal analysis, Investigation, Validation, Visualization, Writing – original draft. **Alice Alipour:** Conceptualization, Funding acquisition, Investigation, Methodology, Project administration, Resources, Supervision, Writing – review & editing.

#### **Declaration of Competing Interest**

The authors declare that they have no known competing financial interests or personal relationships

#### Data availability

Data will be made available on request.

#### References

- De Oliveira A, Silva E, De Medeiros JCP, Loredo-Souza AM, Rocha MM, Rippel LI, Carpeggiani EA, Nunez GLZ. Wind loads on metallic latticed transmission line towers. In: Proceedings of CIGRE Session 2006; 2006.
- [2] Dempsey D, White HB. Winds wreak havoc on lines. Trans Distrib World 1996;48: 32–42.
- [3] Jacobs, M. (2013). 13 of the Largest Power Outages in History and What They Tell us About the 2003 Northeast Blackout. Available at: http://blog.ucsusa.org/2003-north east-blackout-and-13-of-the-largest-power-outages-in-history-199.
- [4] McCarthy P, Melsness M. In: Severe weather elements associated with September 5, 1996 hydro tower failures near Grosse Isle, Manitoba, Canada. Manitoba Environmental Service Centre; 1996. Environment Canada.
- [5] Savory E, Parke GAR, Zeinoddini M, Toy N, Disney P. Modelling of tornado and microburst-induced wind loading and failure of a lattice transmission tower. Eng Struct 2001;23:365–75.
- [6] Zhang W, Zhu J, Liu H, Niu H. Probabilistic capacity assessment of lattice transmission towers under strong wind. Front Built Environ 2015;1. https://doi. org/10.3389/fbuil.2015.00020.
- [7] Ghannoum E. Probabilistic design of transmission lines part I: probability calculations and structural reliability. IEEE Trans Power Appar Syst 1983;102: 3057–64.
- [8] Ghannoum E. Probabilistic design of transmission lines part II: design criteria corresponding to a target reliability. IEEE Trans Power Appar Syst 1983;102: 3065–79.
- [9] American Society of Civil Engineers (ASCE). Guidelines for electrical transmission line structural loading. In: ASCE Manuals and Reports on Engineering Practice, No. 74; 2010.
- [10] European Committee for Electrotechnical Standardization (CENELEC). In: Overhead electrical lines exceeding AC 45 kV. Part 1: General requirements – Common specifications, EN 50341-1; 2001.
- [11] International Electrotechnical Commission (IEC) (2017). Design criteria of overhead transmission line. CEI-60826, Geneva, Switzerland.

- [12] Canadian Standards Association (CSA). Design criteria of overhead transmission line Mississauga. In: Canadian Electrical Code, CSA-C22.3; 2006.
- Dagher HJ, Lu Q. System reliability analysis of transmission lines. Eng Struct 1993;
- [14] Dagher HJ, Kulendran S, Peyrot A, Maamouri M. Relationships between components, structures, and line reliabilities. Probab Methods Appl Electr Power Syst 1991:117-22.
- [15] Foschi RO. Reliability theory and applications to risk analysis of power components and system. Int J Electr Power Energy Syst 2004;26(4):249–56.
- [16] Haldar A. Upgrading of a 230 kV steel transmission line system using probabilistic approach. In: Proceedings of 9thInternational Conference on Probabilistic Methods Applied to Power Systems, PMAPS 2006; 2006.
- [17] Li H, Zhang J, Bhuyan G. Reliability assessment of electrical overhead distribution wood poles. In: International Conference on Probabilistic Methods Applied to Power Systems, PMAPS 2006; 2006.
- [18] Mara TG. Capacity assessment of a transmission tower under wind loading. LondonCanada: University of West Ontario; 2013. Ph.D. dissertation.
- [19] Blevins RD. Applied fluids dynamics handbook. Malabar, FL: Krieger Publishing;
- Georgiou P, Vickery B. Wind loads on building frames. In: Wind Engineering: Proceeding of the Fifth International Conference1; 1979. p. 421-33.
- [21] Lindley D, Willis D. Wind loads on transmission line towers. In: Fifth Australian Conference on Hydraulics and Fluid Mechanics. Christchurch, New Zealand: University of Canterbury; 1974. p. 224-34.
- [22] Whitbread RE. The influence of shielding on the wind forces experienced by arrays of lattice frames. In: Wind Engineering: Proceeding of the Fifth International Conference, vol. 1; 1979. p. 405-20.
- [23] Deng HZ, Xu HJ, Duan CY, Jin XH, Wang ZH. Experimental and numerical study on the responses of a transmission tower to skew incident winds. J Wind Eng 2016;
- [24] Prud'homme S, Legeron F, Langlois S. Calculation of wind forces on lattice structures made of round bars by a local approach. Engineering. Structures 2018; 156:548-55.
- [25] Prud'homme S, Legeron F, Laneville A, Tran MK. Wind forces on single and shielded angle members in lattice structures. J Wind Eng Ind Aerodyn 2014;124:
- [26] Fu X, Li H-N, Li G, Fragility analysis and estimation of collapse status for transmission tower subjected to wind and rain loads. Struct Saf 2016;58:1-10.
- Park H-S, Choi BH, Kim JJ, Lee T-H. Seismic performance evaluation of high voltage transmission towers in South Korea, KSCE J Civ Eng 2016;20(6);2499-505.
- Yang SC, Hong HP, Nonlinear inelastic responses of transmission tower-line system **[28]** under downburst wind. Eng Struct 2016;123:490-500.
- Fu X, Li H-N. Uncertainty analysis of the strength capacity and failure path for a transmission tower under a wind load. J Wind Eng Ind Aerodyn 2018;173:147-55.
- Tian L, Pan H, Ma R, Zhang L, Liu Z. Full-scale test and numerical failure analysis of a latticed steel tubular transmission tower. Eng Struct 2020:208:109919.
- [31] Bi W, Tian L, Li C, Ma Z, Pan H. Wind-induced failure analysis of a transmission tower-line system with long-term measured data and orientation effect. Reliab Eng Syst Saf 2023:229:108875.
- [32] Ma L, Christou V, Bocchini P. Framework for probabilistic simulation of Power Transmission Network performance under hurricanes. Reliab Eng Syst Saf 2022; 217:108072.
- [33] Salman AM, Li Y, Stewart MG. Evaluating system reliability and targeted hardening strategies of power distribution systems subjected to Hurricanes. Reliab Eng Syst Saf 2015:144:319-33.
- [34] Scherb A, Garrè L, Straub D. Evaluating component importance and reliability of power transmission networks subject to windstorms: methodology and application to the Nordic Grid. Reliab Eng Syst Saf 2019;191:106517.

- [35] Xue J, Mohammadi F, Li X, Sahraei-Ardakani M, Ou G, Pu Z. Impact of transmission tower-line interaction to the bulk power system during hurricane. Reliab Eng Syst Saf 2020:203:107079.
- [36] Haldar A, Mahadevan S. Probability, reliability and statistical methods in engineering design. New York, NY: John Wiley; 2000.
- Zhao YG, Ono T. A general procedure for first/second-order reliability method (FORM/SORM). Struct Saf 1999;21:95-112.
- [38] Karamchandani A. Structural system reliability analysis methods. Stanford, California: John A. Blume Earthquake Engineering Center. Department of Civil Engineering. Stanford University; 1987. Report No. 83.
- Melchers RE. Structural reliability analysis and prediction, 2nd edition, UK: Wiley;
- [40] Alipour A, Sarkar P, Dikshit S, Razavi A, Jafari M. Analytical approach to characterize tornado-induced loads on lattice structures. J Struct Eng 2020;146(6).
- Jafari M, Sarkar PP. Wind-induced response characteristics of a yawed and inclined cable in ABL wind: experimental- and numerical-model based study. Eng Struct 2020:214:110681.
- [42] Lu C, Ou Y, Ma X, Je M. Structural analysis of lattice steel transmission towers: a review. J Steel Struct Constr 2016;2(1):1-11.
- [43] Lee P, McClure G. A general three-dimensional L-section beam finite element for elastoplastic large deformation analysis. Comput Struct 2006;84(3-4):215-29.
- [44] Fu X, Li H, Tian L, Wang J, Cheng H. Fragility analysis of transmission line subjected to wind loading. J Perform Constr Facil 2019;33(4):04019044.
- [45] Ozono S, Maeda J. In-plane dynamic interactions between a tower and conductors at lower frequencies. Eng Struct 1992;14(4):210-6.
- [46] JCSS. Probabilistic Model Code-part 3-Material Properties. Joint Committee Struct
- [47] Dolsek M. Incremental dynamic analysis with consideration of modeling uncertainties. Earthq Eng Struct Dyn 2009;38(6):805-25.
- [48] Thomos GC, Trezos CG. Examination of the probabilistic response of reinforced concrete structures under static non-linear analysis. Eng Struct 2006;28(1):120-33.
- Cho IH, Porter K. Modeling building classes using moment matching. Earthq Spectra 2016;32(1):285-301.
- [50] Jahani E, Cetin K, Cho IH. City-scale single family residential building energy consumption prediction using genetic algorithm-based numerical moment matching technique. Build Environ 2020;172:106667.
- [51] Rezaei SN, Chouinard L, Langlois S, A probabilistic framework based on statistical learning theory for structural reliability analysis of transmission line systems. Struct Infrastruct Eng 2017;2479:1-15.
- Sandage KM. A probabilistic analysis for transmission line structures. London: Iowa State University; 1996. M.S. dissertation.

  [53] Shinozuka M, Deodatis G. Simulation of stochastic processes by spectral
- representation. Appl Mech Rev 1991;44(4):191-204.
- Benowitz BA. Deodatis G. Simulation of wind velocities on long span structures: a novel stochastic wave-based model. J Wind Eng Ind Aerodyn 2015;147:154–63.
- [55] Shinozuka M, Jan CM. Digital simulation of random processes and its applications. J Sound Vib 1972;25(1):11-128.
- [56] Benowitz B., Deodatis G. Simulation of wind velocities on long span structures. Safety, Reliability, Risk and Life-Cycle Performance of Structures and Infrastructures 2014:5549-5553
- Haberman R. Applied partial differential equations with Fourier series and boundary value problems. 4th edition, Upper Saddle River, New Jersey: Pearson Prentice Hall: 2004.
- [58] Lee KH, Rosowsky DV. Fragility curves for wood frame structures subjected to lateral wind loads. Wind Struct 2006;9(3):217-30.